ACS Photonics

Letter

Cite This: ACS Photonics 2019, 6, 2649−2654

pubs.acs.org/journal/apchd5

# Donor−Acceptor Distance-Dependent Charge Transfer Dynamics Controlled by Metamaterial Structures

Kwang Jin Lee,[†,□] Yiming Xiao,[‡] Eun Sun Kim,[#] Fabrice Mathevet,[‡] Loic Mager,[§] Olivier Cregut,[§] Frédéric Fages,[∥] Jean-Charles Ribierre,[⊥] Jeong Weon Wu,*[,†,#] and Anthony D'Aléo*[,#,○]

[†]Department of Physics, Ewha Womans University, Seoul 03760, South Korea

[‡]Sorbonne Université, Faculté des Sciences, CNRS, Institut Parisien de Chimie Moléculaire (IPCM), UMR 8232, Chimie des Polymères, 4 Place Jussieu, 75005 Paris, France

[§]CNRS-IPCMS, Université de Strasbourg, 23 Rue du Loess, Strasbourg, France

[∥]Aix Marseille Univ, CNRS, CINaM UMR 7325, Campus de Luminy, Case 913, 13288 Marseille, France

[⊥]Kyushu University, Center for Organic Photonics and Electronics Research, Fukuoka, JP 819-0395, Japan

[#]Center for Quantum Nanoscience, Institute for Basic Science, Seoul 03760, Republic of Korea

[○]Building Blocks for Future Electronics Laboratory (2-B FUEL), The Joint CNRS-Ewha-Yonsei Laboratory, UMI 2002, Seoul, Republic of Korea

[□]Institute of Optics, University of Rochester, Rochester, New York, United States

*Supporting Information*

**ABSTRACT:** The capability to control charge transfer dynamics in a donor−acceptor molecule is important for efficient optoelectronic devices. Charge transfer dynamics is governed by thermodynamics of donor−acceptor charges in a given dielectric environment. Metamaterial structure has been shown to be able to control charge separation and charge recombination processes via nonlocal effect on dielectric permittivity for a fixed donor−acceptor distance organic film. Here, we report the influence of the metamaterial structure on the donor−acceptor distance dependence of the electron transfer process occurring in liquid crystalline organic semiconductor thin films. By examining the charge recombination rate in three different donor−acceptor distances, it is found that the barrier height $\beta$ increases from 0.084 to 0.137 Å$^{-1}$ by 63% in the presence of metal-dielectric multilayered metamaterial structures. Based on the Marcus theory on the charge transfer process, we show that a further increase in the driving force for a larger donor−acceptor distance is mainly responsible for the barrier height increase in the presence of a multilayered metamaterial substrate when compared with a glass substrate. This study will provide a significant step forward in enabling more efficient hybrid organic-optoelectronic devices associated with the charge transfer process.

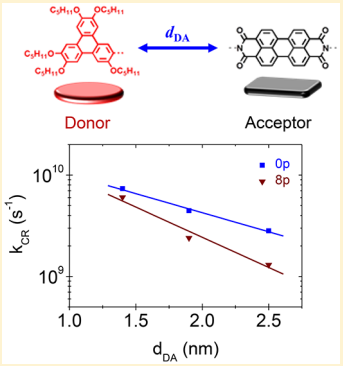


**KEYWORDS:** *organic semiconductors, metamaterials, charge transfer dynamics, nonlocal effect, Marcus theory*



Photoinduced charge transfer in organic molecules is not only a fundamental process in the photosynthesis, but it is also a key primary process in the operation of organic solar cells.[1−8] The ability to promote and control charge transport over long donor (D)−acceptor (A) distances is essential to the development of solar energy conversion systems and molecule-based electronics. Therefore, tuning and controlling the distance-dependent charge transfer (CT) process in D−A molecules has been the focus of a lot of research, motivated by the technological potential in artificial photosynthesis, photovoltaics, and molecular scale electronics.[9,10]

In a molecule composed of D and A, photoinduced charge transfer from D to A leads to a formation of CT state, and a charge recombination (CR) process takes place subsequently. According to the Marcus theory, the CR rate, $k_{CR}$, is associated with the reorganization energy, $\lambda$, and the driving force, $\Delta G$, as well as the electronic D−A coupling, $V_{DA}$.[11] By modulating the CT energy level via dielectric permittivity of the surrounding medium, the CT rate can be controlled locally or nonlocally.[12−16]

For an efficient energy conversion of solar cell devices, a slow CR is desirable,[17−20] and in the solid film structure, a multilayered metamaterial (MM) is an effective means to decrease the $k_{CR}$ of the intramolecular CT state by providing an image−dipole interaction (IDI) of D−A dipoles of the CT state. Owing to IDI, the nonlocal dielectric permittivity of a medium surrounding the CT dipole decreases, leading to an increase in the absolute value of $\Delta G$ for the CR process. As a

**Received:** August 15, 2019
**Published:** November 5, 2019




DOI: 10.1021/acsphotonics.9b01177
ACS Photonics 2019, 6, 2649−2654

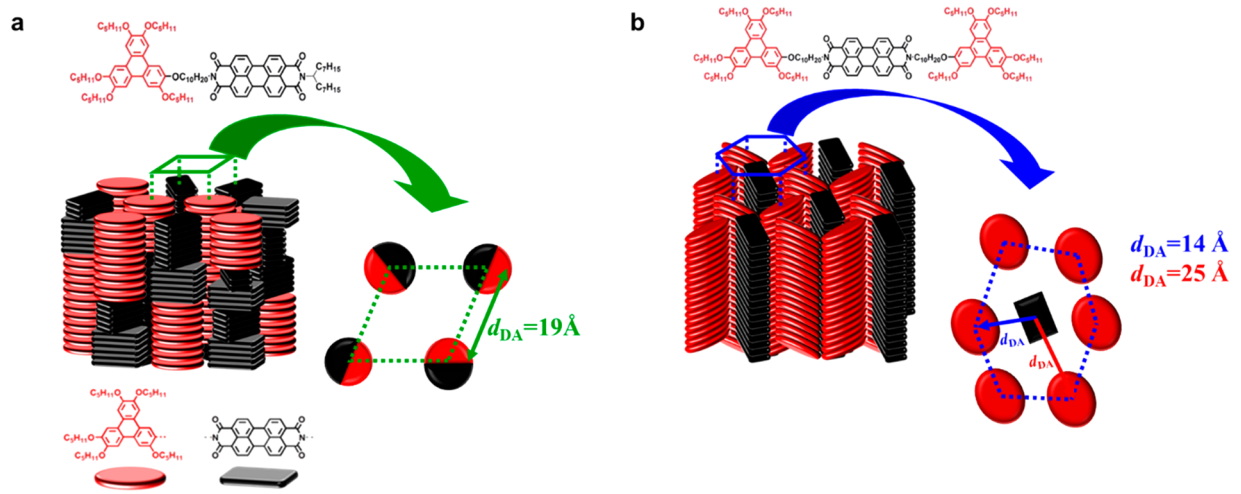


**Figure 1.** Molecular structure and schematic representation of dyad and triad films. (a) Molecular structure of D (triphenylene)−A (perylene diimide) dyad film: the self-organization within the $Col_{hex}$ mesophases and the hexagonal lattice (green dash lozenge) formed by undifferentiated columns. The distance 19 Å corresponds to the average center-to-center spacing between D and A columns ($d_{DA}$). (b) Molecular structure of D−A−D triad film: the self-organization within the $Col_{obl}$ mesophases and the oblique lattice formed by intermingled distinct columns located at the nodes of distorted hexagonal lattices (blue dashed distorted hexagon). The 14 and 25 Å correspond to the two average $d_{DA}$ coexisting within the triad columnar arrangement.

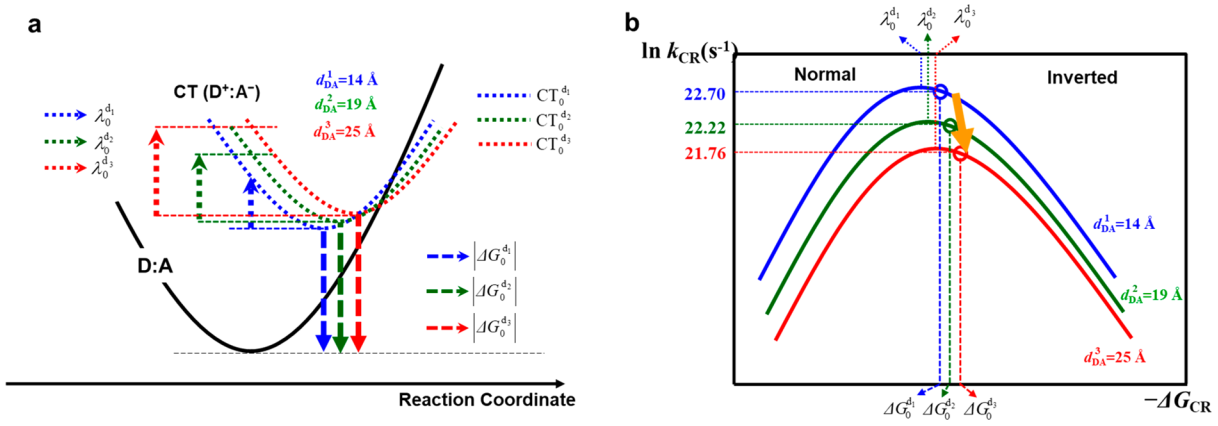


**Figure 2.** CT energy parabolic curve and Marcus parabola for CR process in dyad and triad thin film in the absence of MM structure. (a) CT energy parabola is described in the reaction coordinate. The black parabola of D:A is the ground state of D−A molecule. $CT_n$, $|\Delta G_n|$, and $\lambda_n$ are CT energy parabolic curves, driving force amplitude, and reorganization energy for $d_{DA}$ = 14 Å ($n$ = 1), 19 Å ($n$ = 2), and 25 Å ($n$ = 3), respectively. (b) D−A distance-dependent CR rate is described in terms of Marcus parabola. Yellow arrow indicates that Marcus parabola undergoes a down-right shifting as $d_{DA}$ increases, which leads to a decrease of CR rates, $k_{CR}$. Empty circles correspond to CR rates, $k_{CR}$, for $d_{DA}$ = 14, 19, and 25 Å.

result, when the MM structure is present, $k_{CR}$ can be decreased in the Marcus inverted region with the $\lambda$ unchanged.[15]

Regarding the dependence of $k_{CR}$ on D−A distance, $d_{DA}$, a simple Marcus theory states that $k_{CR}$ exhibits an exponential decay with $d_{DA}$, namely, $k_{CR} = \exp[-\beta \cdot d_{DA}]$, with a barrier height $\beta$ for electron tunneling.[21] However, different examples have been reported, such as $k_{CR}$ reaching the maximum as $d_{DA}$ increases, which was understood in terms of Marcus parabola shifting.[22−24]

In order to identify how the surrounding environment influences the barrier height $\beta$, CT rates have been measured by employing different polarity solvents for D−A molecules with varying $d_{DA}$. Indeed, a local-polarity dependence of $\beta$ has been observed, which is attributed to the fact that the local solvent polarity affects $\lambda$ and $\Delta G$ appearing in the Marcus charge transfer theory.[12−14]

Even though the distance dependence of charge transfer rates has been investigated for decades,[25−32] control of $\beta$ in the D−A molecular system via interaction with a nanophotonic structure has never been studied. In this paper, we examine how the nonlocal effect of MM structure affects the D−A distance-dependent CR rate in dyad and triad organic films. We address how the barrier height $\beta$ depends on the surrounding medium nonlocally in the presence of MM as a local solvent polarity analogue. In the Marcus theory, $\beta$ is a function of the driving force, $\Delta G$, electronic coupling between D and A, $V_{DA}$, and reorganization energy, $\lambda$. Experimental results show that the decrease of $k_{CR}$ with increasing $d_{DA}$ is more pronounced due to a MM structure. In other words, $\beta$ is not a constant parameter, but becomes larger due to a MM structure, resulting from $d_{DA}$-dependent nonlocal dielectric permittivity. Importantly, the capability to modulate $\beta$ by a MM structure nonlocally in a D−A molecular film is of great importance in designing functional charge transfer systems, such as artificial photosynthesis, molecular electronics, and organic photovoltaic devices.



DOI: 10.1021/acsphotonics.9b01177
*ACS Photonics* 2019, 6, 2649−2654

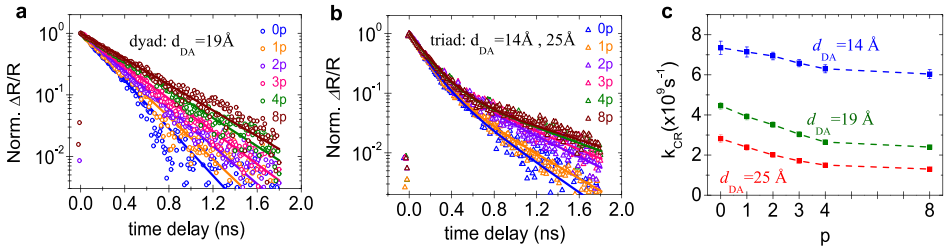


**Figure 3.** Behavior of charge recombination rate in the presence of MM structure. Semilog plot of normalized relative reflection variation ($\Delta R/R$) for (a) dyad and (b) triad thin films on 0*p*, 1*p*, 2*p*, 3*p*, 4*p*, and 8*p* substrates as a function of time delay. Transient absorption decay curves of dyad film are fitted with a monoexponential decay function, while those of triad film are fitted with biexponential decay function to provide two CR time constants. (c) CR rate, $k_{CR}$, is plotted as a function of *p* for $d_{DA}$ = 14, 19, and 25 Å.

In order to study the effect of MM structure in the $d_{DA}$-dependent $k_{CR}$, we adopted a self-assembled discotic liquid-crystalline D−A dyad and D−A−D triad thin films, forming well-separated D and A with $\pi$-stacked columnar structures.[21,33] The structural and self-organization properties of D−A and D−A−D in the solid state are presented in refs 15 and 21. A photoinduced CT process takes place between the triphenylene and perylene bisimide units in both dyad and triad thin films. The chemical structures and schematic representation of the liquid-crystalline dyad and triad molecules that are self-assembled into distinct D and A nanosegregated domains in thin films are presented in Figure 1. For dyad, where a hexagonal lattice is formed by undifferentiated columns, the average $d_{DA}$ is 19 Å, while for triad, where an oblique lattice is formed by intermingled distinct columns located at the nodes of distorted hexagonal lattices, the two different $d_{DA}$ coexisting within the triad columnar arrangement are 14 and 25 Å.[21,33] The bridge between D and A in both dyad and triad is a nonconjugated spacer consisting of 10 carbons.[33]

It is identified that the CR process in organic films of dyad and triad takes place in a Marcus inverted region, as reported in a previous study.[15] Introduction of the Marcus description is briefly presented in the Supporting Information (section II and Figure S1). Based on this, the CT energy level description in the reaction coordinate for dyad and triad films on a glass substrate (without MM structure) with three different $d_{DA}$ is illustrated in Figure 2a. $CT_n$, $|\Delta G_n|$, and $\lambda_n$ are CT energy parabolic curves, driving force amplitude, and reorganization energy for $d_{DA}$ = 14 Å ($n$ = 1), 19 Å ($n$ = 2), and 25 Å ($n$ = 3), respectively. We note that increases of $d_{DA}$ lead to an upward right shift of a CT energy parabola, resulting in $|\Delta G_1| < |\Delta G_2| < |\Delta G_3|$ and $\lambda_1 < \lambda_2 < \lambda_3$. This is in line with the fact that a larger $d_{DA}$ gives rise to a larger $|\Delta G|$ and $\lambda$.[23] Figure 2b displays the Marcus parabola that describes how $k_{CR}$ changes with $d_{DA}$. A yellow arrow indicates that the downward-right shift of the Marcus parabola with increasing $d_{DA}$ results in a decrease in $k_{CR}$[23,24] and exhibits the same relationship of $|\Delta G_1| < |\Delta G_2| < |\Delta G_3|$ and $\lambda_1 < \lambda_2 < \lambda_3$ as what Figure 2a shows. This is also consistent with the fact that the CR process in the present D−A molecular system takes place in the Marcus inverted region.[15]

The MM structures consist of 10 nm thick Ag and $Al_2O_3$ alternative layers deposited on a glass substrate by means of electron beam evaporation with different numbers of Ag−$Al_2O_3$ pairs. Since $Al_2O_3$ is a perfect insulating material with a large bandgap energy (~7 eV), it can block any type of charge transport processes between a metal and an organic semiconductor. We denote that *p* is the number of Ag−$Al_2O_3$ pairs. After that, 40 nm thick films of dyad/triad were spin-coated on top of the MM substrates with 0*p*, 1*p*, 2*p*, 3*p*, 4*p*, and 8*p*. 0*p* means a glass substrate without MM. That is, six thin film samples are prepared for dyad and triad, respectively. A TEM image of a four-pair MM structure, as well as the linear optical spectra of the MM structure for each metal−dielectric pair, and dielectric constants of 10 nm thick Ag and $Al_2O_3$ layer are presented in Figure S3 of the Supporting Information.

The femtosecond transient absorption (TA) experiments have been carried out to measure CR rates of D−A molecules with $d_{DA}$ = 14 Å (triad), 19 Å (dyad), and 25 Å (triad) in dyad and triad thin films deposited on 0*p*, 1*p*, 2*p*, 3*p*, 4*p*, and 8*p* MM structures by measuring a relative reflection ($\Delta R/R$). The 325 nm pump and 725 nm probe beams were used to monitor the CR dynamics of the dyad and triad films based on their linear absorption (Figure S3) and CT properties.[21] Detailed information on TA measurements is presented in the SI.

Figure 3 presents the CR dynamics of the dyad and triad thin films with MM substrates. Raw data of $\Delta R/R$ for dyad and triad films were fitted with monoexponential and biexponential decay curves, respectively.[15,21] After that, we normalized the whole data including fit curves as shown in Figure 3a,b. For dyad film with $d_{DA}$ = 19 Å, we obtain the ratio value, $k_{CR}$ (8*p*)/$k_{CR}$ (0*p*), of 0.53 (Figure S4 and Table S1). We note that the TA decay curve of the triad film was not fitted with a monoexponential decay, but with a biexponential decay function, since the triad film possesses two different $k_{CR}$.[21] For 0*p* substrate, we obtain the same results as those reported in the previous work within the experimental error. The ratio values, $k_{CR}(8p)/k_{CR}(0p)$, are obtained to be 0.82 and 0.45 for $d_{DA}$ = 14 and 25 Å, respectively (Figure S4 and Table S1). In Figure 3c, we plot the $k_{CR}$ as a function of the number of *p*. We note that the change in $k_{CR}$ becomes larger as $d_{DA}$ increases for $d_{DA}$ = 14 Å (triad), 19 Å (dyad), and 25 Å (triad). Entire data of $k_{CR}$ as a function of *p* for three different $d_{DA}$ is summarized in Table 1.

**Table 1. Summarization of $k_{CR}$ for $d_{DA}$ = 14, 19, and 25 Å in the Presence of MM Structures of 0*p*, 1*p*, 2*p*, 3*p*, 4*p*, and 8*p***

| No. of pairs | $k^1_{CR}$ (×10$^9$ s$^{-1}$; $d_1$ = 14 Å) | $K^2_{CR}$ (×10$^9$ s$^{-1}$; $d_2$ = 19 Å) | $K^3_{CR}$ (×10$^9$ s$^{-1}$; $d_3$ = 25 Å) |
|---|---|---|---|
| 0*p* | 7.35 ± 0.33 | 4.46 ± 0.23 | 2.82 ± 0.18 |
| 1*p* | 7.14 ± 0.25 | 3.92 ± 0.21 | 2.39 ± 0.15 |
| 2*p* | 6.94 ± 0.20 | 3.51 ± 0.19 | 2.01 ± 0.13 |
| 3*p* | 6.58 ± 0.18 | 3.04 ± 0.13 | 1.71 ± 0.12 |
| 4*p* | 6.37 ± 0.17 | 2.67 ± 0.15 | 1.46 ± 0.10 |
| 8*p* | 6.06 ± 0.13 | 2.40 ± 0.11 | 1.28 ± 0.10 |



DOI: 10.1021/acsphotonics.9b01177
ACS Photonics 2019, 6, 2649−2654

We also have measured the charge separation (CS) rates $k_{CS}$ as a function of the number of $p$. Both dyad and triad films exhibited a slowing down of CS rate as $p$ increases. However, two different CS rates of D−A molecules with $d_{DA}$ = 14 and 25 Å could not be identified since the CS rates are in the order of hundreds of femtosecond (Figure S5).

In Figure 4a, among the data of $k_{CR}$ versus $d_{DA}$ for six different metal−dielectric pairs, we semilog plot $k_{CR}$ as a function of $d_{DA}$ for 0$p$ and 8$p$ substrates with the slope $\beta$ in the absence (0$p$) and presence (8$p$) of the MM structure. Notably, we find that $\beta$ increases significantly from 0.084 Å$^{-1}$ to 0.137 Å$^{-1}$ for 0$p$ and 8$p$ substrates, respectively, which corresponds to 63% increase of $\beta$ in the presence of 8$p$ MM structure. In order to examine how the number of metal−dielectric pairs of MM modulates the barrier height, the behavior of $\beta$ as a function of $p$ is plotted in Figure 4b. We find that the change of $\beta$ with $p$ is not linear, but clearly saturated as $p$ increases, which is also in accord with the previous theoretical analysis that the IDI effect converges to a finite quantity with $p$ increasing (Figure S6).[15]

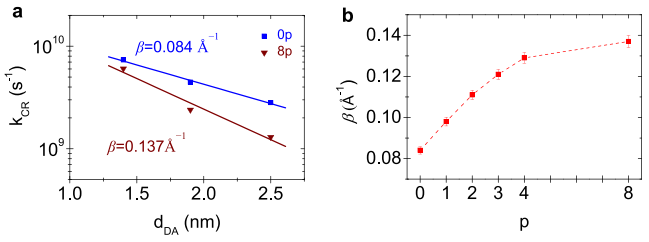


**Figure 4.** Increase of barrier height $\beta$ in the presence of MM structures. (a) Semilog plot of $k_{CR}$ as a function of $d_{DA}$ for 0$p$ and 8$p$ substrates. $\beta$ = 0.084 Å$^{-1}$ and 0.137 Å$^{-1}$ for 0$p$ and 8$p$ substrates, respectively. Data for other numbers of metal−dielectric pairs are reported in the Supporting Information. (b) The barrier height $\beta$ is plotted as a function of the number of metal−dielectric pairs, $p$. The increase of barrier height is saturated upon increasing $p$.

As we mentioned before, according to Marcus theory, electron transfer rate is mainly governed by $V_{DA}$, $\Delta G$, and $\lambda$ with fixed temperature ($T$). The semiclassical Marcus theory can be written as[11]

$$k_{CR} = \sqrt{\frac{\pi}{\hbar^2 \lambda k_B T}} V_{DA}^2 \exp\left[-\frac{(\lambda + \Delta G_{CR})^2}{4\lambda k_B T}\right] \quad (1)$$

where $\hbar$ and $k_B$ are the Planck constant and the Boltzmann constant, respectively. For fixed $\Delta G$ and $\lambda$, exponential dependence of $k_{CR}$ on $d_{DA}$ is attributed to the exponential dependence of $V_{DA}$ on $d_{DA}$. As $d_{DA}$ changes, however, both $\Delta G$ and $\lambda$ can also contribute to a change in CT dynamics since they are dependent on $d_{DA}$ (eq S2 and S2 in the Supporting Information). This can be understood in terms of shift of CT energy parabola in reaction coordinate and Marcus parabola for different $d_{DA}$ in the absence of MM structure (Figure 2).

Therefore, we adopt the Marcus theory to explain the experiment data of the $d_{DA}$ dependent CR rates for a different number of metal−dielectric pairs of MM substrate. In Figure 5, we describe the energy parabolas of ground and CT states in the reaction coordinates. The black parabolic curve of D:A and the colored parabolic curves of D$^+$:A$^-$ correspond to the ground state and CT state of D−A molecule, respectively. Two solid and dashed curves describe the CT states for $d_1$ = 14 Å (blue) and $d_3$ = 25 Å (red) in the absence and presence of MM structures, respectively. We find that CT energy parabolic curves undergo upward shifting in the presence of MM structure, resulting from the decrease of nonlocal dielectric permittivity, while there is no change along horizontal reaction coordinate.[15]

We also show that CT energy parabolic curve moves upward as $d_{DA}$ increases, which is plotted as blue ($d_{DA}$ = 14 Å) and red ($d_{DA}$ = 25 Å) dotted CT energy parabolic curves (the color code the same as that in Figure 1a). In the presence of MM structure, CT energy parabolic curves move upward for a fixed $d_{DA}$, which is from a nonlocal dielectric permittivity.[15] Importantly, the increase in the CT energy level due to a

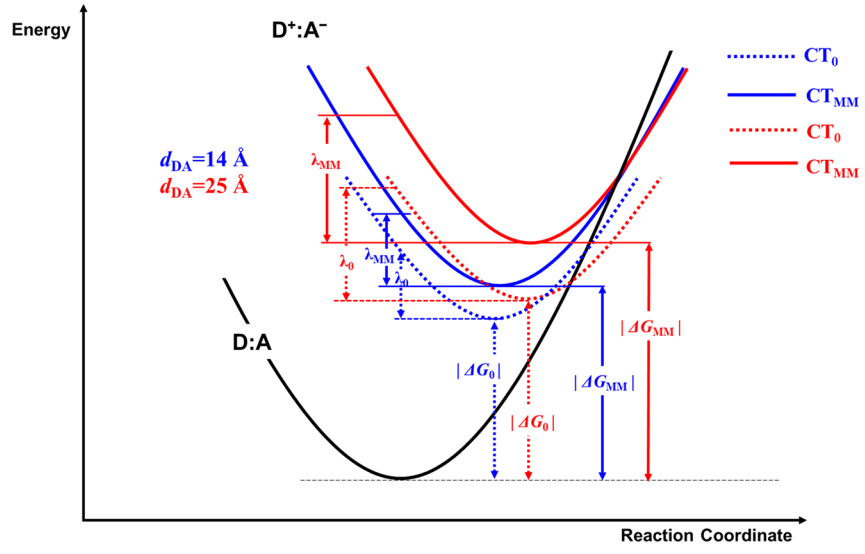


**Figure 5.** CT energy parabolic curve description in the presence of MM substrate. Energy parabola describing the CT process is illustrated in the reaction coordinate. The black parabola of D:A is the ground state of D−A molecule while blue and red solid (dotted) parabolas are the CT states in the presence (absence) of MM structure for $d_{DA}$ = 14 and 25 Å, respectively. The amplitude of driving force and reorganization energy are denoted as $|\Delta G_{MM}|$ ($|\Delta G_0|$) and $\lambda_{MM}$ ($\lambda_0$) in the presence (absence) of the MM structure for $d_{DA}$ = 14 Å (blue) and 25 Å (red).



DOI: 10.1021/acsphotonics.9b01177
ACS Photonics 2019, 6, 2649−2654

nonlocal effect is more pronounced for larger $d_{DA}$, as can be seen by comparing dotted (0$p$) and solid (8$p$ MM) CT energy parabolas of blue ($d_{DA}$ = 14 Å) and red ($d_{DA}$ = 25 Å) colors. This important fact originates from the fact that IDI effect gets stronger for a larger $d_{DA}$, since the CT dipole strength is proportional to $d_{DA}$. The entire CT energy parabola description, including $d_{DA}$ = 19 Å, is displayed in Figure S7 of the Supporting Information.

We note that $\Delta G$ depends on the static dielectric permittivity, as shown in eq S1 (Supporting Information). Consequently, due to a MM structure, CT energy level can be modulated by nonlocal effect on the dielectric permittivity based on IDI, which leads to (1) slowing down of CR rate due to the increase of driving force in the inverted region and (2) blue shifting of CT emission when CT emitter is located nearby MM structure.[15,16]

On the other hand, we should keep in mind that the $d_{DA}$ dependence of $V_{DA}$ is not taken into account in the energy level diagram of Figure 5. In order to examine the behavior of $k_{CR}$ more detail, we employ the Marcus parabola description based on eq 1 in which $k_{CR}$ exhibits a Gaussian free energy dependence, resulting in a parabola shape when $\ln(k_{CR})$ is plotted as a function of $-\Delta G_{CR}$. We note that the exponential decay of $k_{CR}$ as a function of $d_{DA}$ is mainly from the fact that $V_{DA}$ decreases exponentially with $d_{DA}$. Hence, in Figure 6, the Marcus parabolas shift downward with increasing $d_{DA}$. The parabola also shifts to the right as $d_{DA}$ increases since maximal $k_{CR}$ is reached at the point satisfying $-\Delta G_{CR} = \lambda$.

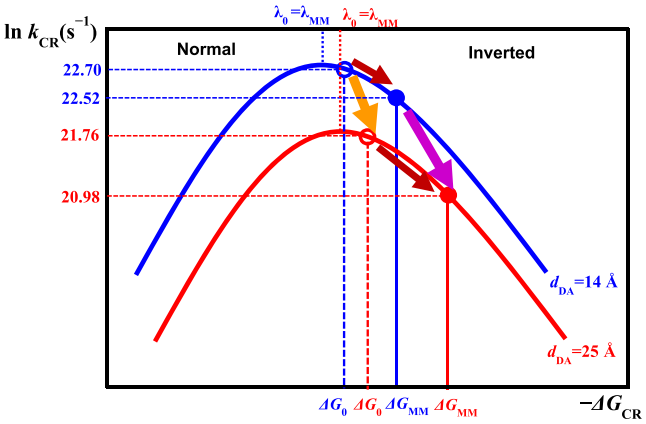


**Figure 6.** Marcus parabola for CR process in dyad and triad thin film on MM substrate. D−A distance dependent CR rate is described in terms of Marcus parabola. Empty and filled circles correspond to CR rates, $k_{CR}$, in the absence and presence of MM substrate, respectively. The yellow (sky blue) arrow shows the decrease of $k_{CR}$ as $d_{DA}$ increases from 14 to25 Å in the absence (presence) of MM structure, where the decrease of CR rate is more pronounced in the presence of MM structure.

In Figure 6, empty (filled) circles indicate the $k_{CR}$ when in the absence (presence) of MM structures, where Marcus parabolas for three different $d_{DA}$ display a down-right shifting. Yellow and blue arrows indicate a decreasing behavior of $k_{CR}$ with $d_{DA}$ in both the absence and the presence of MM since $V_{DA}$ is proportional to $\exp[-\beta \cdot d_{DA}]$, irrespective of the presence of MM. A yellow arrow depicts that $|\Delta G|$ increases with $d_{DA}$, which is in line with the Figure 5. The blue arrow depicts a slowing down of $k_{CR}$ due to the MM structure, indicating that $k_{CR}$ decreases more as $d_{DA}$ becomes larger. This is manifested to a longer blue arrow than a yellow arrow, which eventually shows that $\beta$ becomes larger in the presence of the MM structure. We note that $\lambda$ increases with $d_{DA}$, but for fixed $d_{DA}$, it remains constant, regardless of the presence of the MM structures. Overall qualitative trends of $\lambda$ and $\Delta G$ are in line with Figure 5, showing that both the amplitude of $\lambda$ and $\Delta G$ are increased as $d_{DA}$ increases in the presence of MM structures. Entire Marcus parabola description including $d_{DA}$ = 19 Å is displayed in Figure S8 of the Supporting Information.

It is worth noting that Wenger and co-worker reported that the electron transfer rate reaches maxima at certain $d_{DA}$, which was explained by a relatively weak distance dependence of $V_{DA}$ combined with a strong increase of the $\lambda$ with increasing $d_{DA}$.[23] This kind of nonmonotonic behavior can take place only in Marcus inverted region when the degree of lateral movement of Marcus parabola by the change in $\lambda$ is greater than the vertical movement for different $d_{DA}$. This shows that distance-dependent CT rate is relatively more complex to describe in a simple exponential decay approach. In our case, however, we did not obtain nonmonotonic behavior, which means that the $V_{DA}$ would be comparable to the $d_{DA}$ dependence of $\lambda$ and, therefore, could not allow the maximum point of electron transfer rate.

In conclusion, we have investigated the influence of MM structure on distance-dependent photoinduced charge transfer dynamics in self-organized liquid crystalline dyad and triad molecules with nonconjugated spacers in which three different D−A distances exist. We found that the barrier height $\beta$ increases significantly by 60% due to a MM structure, which is understood in terms of Marcus theory framework by taking into account both the nonlocal effect on dielectric environment and the variation of reorganization energy with varying D−A distance. This enhancement of $\beta$ shows the possibility of actively controlling the barrier height via nonlocal effect of MM structures and will pave the way for development of new applications such as organic optoelectronic devices.

## ■ ASSOCIATED CONTENT

### Supporting Information

The Supporting Information is available free of charge on the ACS Publications website at DOI: 10.1021/acsphotonics.9b01177.

Detailed femtosecond transient absorption measurement based on pump−probe technique and supplemental data (PDF)

## ■ AUTHOR INFORMATION


### Corresponding Authors

*E-mail: jwwu@ewha.ac.kr.
*E-mail: anthony.daleo@cnrs.fr.

### ORCID

Kwang Jin Lee: 0000-0002-3200-8264
Frédéric Fages: 0000-0003-2013-0710
Jean-Charles Ribierre: 0000-0001-7288-3795
Jeong Weon Wu: 0000-0001-7027-841X


### Notes

The authors declare no competing financial interest.



DOI: 10.1021/acsphotonics.9b01177
ACS Photonics 2019, 6, 2649−2654

## ■ ACKNOWLEDGMENTS

This work is supported by funding of the Ministry of Science, ICT & Future Planning, Korea (2014M3A6B3063708, 2017R1E1A1A01075394).

## ■ REFERENCES

(1) Song, P.; Li, Y.; Ma, F.; Pullerits, T.; Sun, M. Photoinduced Electron Transfer in Organic Solar Cells. *Chem. Record.* **2016**, *16*, 734−753.
(2) Fukuzumi, S.; Ohkubo, K.; Suenobu, T. Long-Lived Charge Separation and Applications in Artificial Photosynthesis. *Acc. Chem. Res.* **2014**, *47*, 1455−1464.
(3) Vandewal, K.; Albrecht, S.; Hoke, E. T.; Graham, K. R.; Widmer, J.; Douglas, J. D.; Schubert, M.; Mateker, W. R.; Bloking, J. T.; Burkhard, G. F.; Sellinger, A.; Fréchet, J. M. J.; Amassian, A.; Riede, M. K.; McGehee, M. D.; Neher, D.; Salleo, A. Efficient charge generation by relaxed charge-transfer states at organic interfaces. *Nat. Mater.* **2014**, *13*, 63−68.
(4) Gélinas, S.; Rao, A.; Kumar, A.; Smith, S. L.; Chin, A. W.; Clark, J.; van der Poll, T. S.; Bazan, G. C.; Friend, R. H. Ultrafast long-range charge separation in organic semiconductor photovoltaic diodes. *Science* **2014**, *343*, 512−517.
(5) Liu, H.; Bai, Q.; Yao, L.; Zhang, H.; Xu, H.; Zhang, S.; Li, W.; Gao, Y.; Li, J.; Lu, P.; Wang, H.; Yang, B.; Ma, Y. Highly efficient near ultraviolet organic light-emitting diode based on a meta-linked donor−acceptor molecule. *Chem. Sci.* **2015**, *6*, 3797−3804.
(6) Deotare, P. B.; Chang, W.; Hontz, E.; Congreve, D. N.; Shi, L.; Reusswig, P. D.; Modtland, B.; Bahlke, M. E.; Lee, C. K.; Willard, A. P.; Bulović, V.; Van Voorhis, T.; Baldo, M. A. Nanoscale transport of charge-transfer states in organic donor-acceptor blends. *Nat. Mater.* **2015**, *14*, 1130−1134.
(7) Brédas, J.; Beljonne, D.; Coropceanu, V.; Cornil, J. Charge-Transfer and Energy-Transfer Processes in π-Conjugated Oligomers and Polymers: A Molecular Picture. *Chem. Rev.* **2004**, *104*, 4971−5002.
(8) Veldman, D.; Meskers, S. C. J.; Janssen, R. A. J. The Energy of Charge-Transfer States in Electron Donor−Acceptor Blends: Insight into the Energy Losses in Organic Solar Cells. *Adv. Funct. Mater.* **2009**, *19*, 1939−1948.
(9) Wasielewski, M. R. Self-Assembly Strategies for Integrating Light Harvesting and Charge Separation in Artificial Photosynthetic Systems. *Acc. Chem. Res.* **2009**, *42*, 1910−1921.
(10) Tavernier, H. L.; Fayer, M. D. Distance Dependence of Electron Transfer in DNA: The Role of the Reorganization Energy and Free Energy. *J. Phys. Chem. B* **2000**, *104*, 11541−11550.
(11) Marcus, R. A. Electron transfer reactions in chemistry. Theory and experiment. *Rev. Mod. Phys.* **1993**, *65*, 599.
(12) Oswald, F.; Shafiqul Islam, D.-M.; El-Khouly, M. E.; Araki, Y.; Caballero, R.; de la Cruz, P.; Ito, O.; Langa, F. Photoinduced electron transfer of zinc porphyrin−oligo(thienylenevinylene)−fullerene[60] triads; thienylenevinylenes as efficient molecular wires. *Phys. Chem. Chem. Phys.* **2014**, *16*, 2443−2451.
(13) Nakamura, T.; Fujitsuka, M.; Araki, Y.; Ito, O.; Ikemoto, J.; Takimiya, K.; Aso, Y.; Otsubo, T. Photoinduced Electron Transfer in Porphyrin-Oligothiophene-Fullerene Linked Triads by Excitation of a Porphyrin Moiety. *J. Phys. Chem. B* **2004**, *108*, 10700−10710.
(14) Luo, Y.; Barthelmes, K.; Wächtler, M.; Winter, A.; Schubert, U. S.; Dietzek, B. Increased Charge Separation Rates with Increasing Donor−Acceptor Distance in Molecular Triads: The Effect of Solvent Polarity. *J. Phys. Chem. C* **2017**, *121*, 9220−9229.
(15) Lee, K. J.; Xiao, Y.; Woo, J. H.; Kim, E.; Kreher, D.; Attias, A.-J.; Mathevet, F.; Ribierre, J.-C.; Wu, J. W.; André, P. Charge-transfer dynamics and nonlocal dielectric permittivity tuned with metamaterial structures as solvent analogues. *Nat. Mater.* **2017**, *16*, 722−730.
(16) Lee, K. J.; Lee, Y. U.; Fages, F.; Ribierre, J.-C.; Wu, J. W.; D'Aléo, A. Blue-Shifting Intramolecular Charge Transfer Emission by Nonlocal Effect of Hyperbolic Metamaterials. *Nano Lett.* **2018**, *18*, 1476−1482.
(17) Deibel, C.; Strobel, T.; Dyakonov, V. Role of the Charge Transfer State in Organic Donor−Acceptor Solar Cells. *Adv. Mater.* **2010**, *22*, 4097−4111.
(18) Guo, J.; Ohkita, H.; Benten, H.; Ito, S. Charge Generation and Recombination Dynamics in Poly(3-hexylthiophene)/Fullerene Blend Films with Different Regioregularities and Morphologies. *J. Am. Chem. Soc.* **2010**, *132*, 6154−6164.
(19) Clarke, T. M.; Durrant, J. R. Charge photogeneration in organic solar cells. *Chem. Rev.* **2010**, *110*, 6736−6767.
(20) Lakhwani, G.; Rao, A.; Friend, R. H. Bimolecular recombination in organic photovoltaics. *Annu. Rev. Phys. Chem.* **2014**, *65*, 557−581.
(21) Lee, K. J.; Woo, J. H.; Xiao, Y.; Kim, E.; Mazur, L. M.; Kreher, D.; Attias, A.-J.; Matczyszyn, K.; Samoc, M.; Heinrich, B.; Méry, S.; Fages, F.; Mager, L.; D'Aléo, A.; Wu, J. W.; Mathevet, F.; André, P.; Ribierre, J.-C. Structure−charge transfer property relationship in self-assembled discotic liquid-crystalline donor−acceptor dyad and triad thin films. *RSC Adv.* **2016**, *6*, 57811−57819.
(22) Kuss-Petermann, M.; Wenger, O. S. Increasing Electron-Transfer Rates with Increasing Donor−Acceptor Distance. *Angew. Chem., Int. Ed.* **2016**, *55*, 815−819.
(23) Kuss-petermann, M.; Wenger, O. S. Electron transfer rate maxima at large donor−acceptor distances. *J. Am. Chem. Soc.* **2016**, *138*, 1349−1358.
(24) Kuss-Petermann, M.; Wenger, O. S. Unusual distance dependences of electron transfer rates. *Phys. Chem. Chem. Phys.* **2016**, *18*, 18657−18664.
(25) Oevering, H.; Paddon-Row, M. N.; Heppener, M.; Oliver, A. M.; Cotsaris, E.; Verhoeven, J. W.; Hush, N. S. Long-range photoinduced through-bond electron transfer and radiative recombination via rigid nonconjugated bridges: distance and solvent dependence. *J. Am. Chem. Soc.* **1987**, *109*, 3258−3269.
(26) Schanze, K. S.; Sauer, K. Photoinduced intramolecular electron transfer in peptide-bridged molecules. *J. Am. Chem. Soc.* **1988**, *110*, 1180−1186.
(27) Moser, C. C.; Keske, J. M.; Warncke, K.; Farid, R. S.; Dutton, P. L. Nature of biological electron transfer. *Nature* **1992**, *355*, 796−802.
(28) Edwards, P. P.; Gray, H. B.; Lodge, M. T. J.; Williams, R. J. P. Electron Transfer and Electronic Conduction through an Intervening Medium. *Angew. Chem., Int. Ed.* **2008**, *47*, 6758−6765.
(29) Lukacs, A.; Eker, A. P. M.; Byrdin, M.; Brettel, K.; Vos, M. H. Electron Hopping through the 15 Å Triple Tryptophan Molecular Wire in DNA Photolyase Occurs within 30 ps. *J. Am. Chem. Soc.* **2008**, *130*, 14394−14395.
(30) Cordes, M.; Giese, B. Electron transfer in peptides and proteins. *Chem. Soc. Rev.* **2009**, *38*, 892−901.
(31) Winkler, J. R.; Gray, H. B. Long-Range Electron Tunneling. *J. Am. Chem. Soc.* **2014**, *136*, 2930−2939.
(32) O'Hanlon, D. C.; Cohen, B. W.; Moravec, D. B.; Dallinger, R. F.; Hopkins, M. D. Electronic, Redox, and Photophysical Consequences of Metal-for-Carbon Substitution in Oligo-Phenylene-Ethynylenes. *J. Am. Chem. Soc.* **2014**, *136*, 3127−3136.
(33) Xiao, Y.; Su, X.; Sosa-Vargas, L.; Lacaze, E.; Heinrich, B.; Donnio, B.; Kreher, D.; Mathevet, F.; Attias, A.-J. Chemical engineering of donor−acceptor liquid crystalline dyads and triads for the controlled nanostructuration of organic semiconductors. *CrystEngComm* **2016**, *18*, 4787−4798.



DOI: 10.1021/acsphotonics.9b01177
*ACS Photonics* 2019, 6, 2649−2654